Nuclear Inst. and Methods in Physics Research, A 994 (2021) 165044

Contents lists available at ScienceDirect

Nuclear Inst. and Methods in Physics Research, A

journal homepage: www.elsevier.com/locate/nima

Hardware based contrast enhancement and cupping reduction in industrial MeV Cone Beam Computed Tomography

Carina von Deschwanden [a,1], Richard Schielein [b], Mathieu Plamondon [a,2], Jürgen Hofmann [a], Alexander Flisch [a,*], Stefan Kasperl [b], Randolf Hanke [b,c], Alex Dommann [a]

[a] Empa, Swiss Federal Laboratories for Materials Science and Technology, Center for X-ray Analytics, Überlandstrasse 129, 8600 Dübendorf, Switzerland
[b] Fraunhofer Development Center for X-ray Technology EZRT, Flugplatzstr. 75, 90768 Fürth, Germany
[c] Chair of X-ray Microscopy, University Würzburg, Josef-Martin-Weg 63, 97074 Würzburg, Germany

ARTICLE INFO

Keywords:
X-ray
Computed Tomography
High energy application
Monte-Carlo simulation

ABSTRACT

This work investigates a detector sided filter concept for contrast enhancement and cupping reduction in an industrial Mega Electronvolt (MeV) Cone Beam Computed Tomography (CBCT) system employing a 6 MeV linear accelerator source and a commercial Gadox based flat panel imager. The method was evaluated using a steel step cylinder sample in order to test the efficiency of the hardware based improvement for various material transmission lengths. An overall improvement of the reconstructed signal for the suggested detector filter configurations with respect to the non-filtered measurements can be observed. Furthermore, equivalent source sided filtrations are shown to be less effective than their detector sided counterpart. Of the detector filter configurations studied in this work, a 2 mm lead filter caused the maximal contrast enhancement, while a 5 mm copper filter lead to better results with regard to cupping artefact reduction.

1. Introduction

Industrial X-ray Computed Tomography (CT) is a non-destructive inspection technique for the investigation of the structure and interior features of objects. For the measurement of large and dense objects, a high energy X-ray source operating at energies exceeding one Mega-Electronvolt (MeV) is necessary in order to achieve sufficient X-ray transmission. High energy (HE) industrial X-ray CT setups primarily employ a linear accelerator as a source which is typically combined with a line detector. This line detector can be operated with either a narrow slit collimator or even a row of individually collimated detector channels. This so-called fan-beam setup helps to reduce the total amount of scattered radiation in the measured signal improving the overall signal quality.

Current lower energetic X-ray CT setups operating at energies up to several hundred kilo electronvolt (keV) are designed in the so-called cone-beam geometry. The two-dimensional flat panel imagers in these systems are based on either scintillation crystals or phosphors, which convert the incident radiation into visible light. A photodetector is able to convert these optical photons into an electrical signal. The significant increase in resolution and inspection speed lead to the great success of the cone-beam measurement method over the fan-beam applications.

Unfortunately, the non-negligible amount of single and multiple scattered radiation at high X-ray energies rendered MeV Cone-Beam CT (CBCT) measurements impossible [1,2]. Furthermore, the design of commercial flat panel detectors leads to low and non-linear conversion of the incident radiation into a signal. These two aspects cause a significant decrease in contrast and signal strength especially for the high energy photons. This phenomenon is called the absorption and quantum noise of the setup, which has been previously studied in Monte Carlo (MC) simulations for MeV X-ray absorption radiography [3].

The use of filter material to amend image degrading effects and to enhance detection has been studied in the field of X-ray detection before. In the medical field of radiotherapy, layered materials in combination with high energy X-ray sources were investigated. Particularly the change in conversion noise of high energy radiation in order to increase the accuracy of dose measurements and treatment planning was of interest. Moreover, in intensity modulated radiotherapy (IMRT) different layers of materials are used to increase the sensitivity of an imager at high energies [4]. In high energy X-ray dosimetry applications, these materials inserted in front of the detector are known as build-up layers. Their main purpose is to increase the accuracy of dose measurements [5].

In the field of non-destructive testing filtration is typically employed at the source. The pre-filtering of the beam aims to increase its mean

* Corresponding author.
E-mail address: alexander.flisch@empa.ch (A. Flisch).
[1] Currently at Bisikonerstrasse 1, 8307 Effretikon, Switzerland.
[2] Currently at Varian Medical Systems Inc., 5405 Baden-Dättwil, Switzerland.

https://doi.org/10.1016/j.nima.2021.165044
Received 22 July 2020; Received in revised form 13 November 2020; Accepted 8 January 2021
Available online 30 January 2021

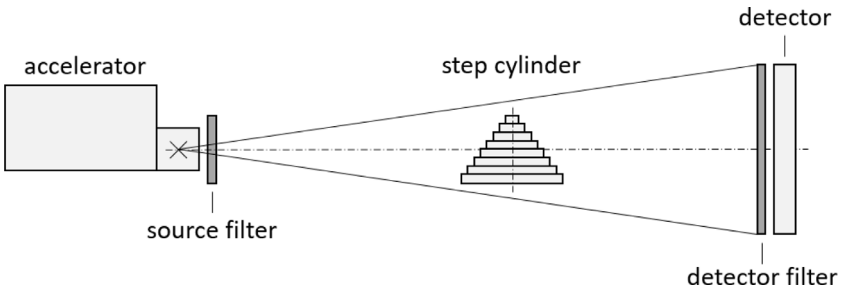

Fig. 1. Setup of the MeV CBCT system showing the main components and the position of the filters.

energy and cut off the low energy part of the spectrum. This method decreases the effects of beam hardening, reducing artefacts such as cupping in the reconstructed volume [6]. However, detector sided filtration was also in use, specifically for inspections using X-ray films [7]. Here, the filter material is employed for the reduction of scattered radiation in the measured signal.

In this work, we inspect detector sided filtration in the context of industrial MeV CBCT measurements of large and dense specimens. This work is based on the dissertation of Stritt [8]. The filter material at the detector should improve the efficiency and contrast of the HE CBCT measurements by increasing the number of detected photons of the imager at high energies with the help of so-called close force scattering events. These enforced scattering events in the filter material give rise to a lower energy scatter cone, which is more likely to be detected by the imagers scintillation layer. A simultaneous decrease of object scattered radiation in the signal achieved by filtering out a significant amount of incident low energy radiation will lead to an increase in signal quality. An evaluation of several filter materials and various thicknesses with respect to their impact on X-ray images and detection efficiency is performed. Additional MC simulations help to understand the impact of the filter material on the scatter-to-primary ratio (SPR), the mean energy of the beam and the energy dependent detection efficiency of the detector.

2. Experimental setup

The high energy industrial cone beam CT setup studied in this work consists of a linear accelerator capable of producing an X-ray beam with a 4 or 6 MeV spectrum. The radiation is generated in a 0.85 mm thick tungsten transmission target and the focal spot size of the source has a diameter of 2 mm. The detector employed in the X-ray CBCT setup is a flat panel imager from Perkin Elmer, model XRD1621 with a pixel size of 200 µm [9], which is placed at a distance of 4.5 m from the source. An additional shielding of 60 mm thick lead plates was installed in order to protect the electronics of the detector from the high energy X-ray radiation. The shielding reduces the detection area of the imager by 25 mm at each side leading to a detection area of 359.6 mm × 359.6 mm, which corresponds to a matrix of 1798 × 1798 pixels. Detailed information about the system components of the MeV CBCT setup can be found in Table 1. Table 2 shows the acquisition parameters for the source and the detector used in the measurements. The filters studied in this work were set up either at the source or in front of the detector. The distance between the source and the filter as well as between the filter and the detector were chosen to be as small as possible. As a result the source filters were placed after the primary source collimator in a distance of 63 mm to the X-ray target. Moreover, the detector sided filters were mounted directly on the entrance window of the detector. The setup of the MeV CBCT system is shown in Fig. 1.

In order to study the effects of scattered radiation and beam hardening for different transmission lengths a step cylinder made of stainless steel was chosen as a test object. This step cylinder consists of eight hollow steel cylinders of 20 mm height with an inner hole diameter of 20 mm. The outer diameters of the eight cylinders are 40, 60, 80, 100, 120, 160, 200 and 220 mm respectively. An image of this step cylinder can be found in Fig. 2 and a schematic drawing in Fig. 3.

Each scan was performed with 1600 projections and with 4 frames averaged per projection. The integration time per frame was adjusted depending on the filter configuration in order to utilize the full dynamic range of the detector. Integration times per frame for each corresponding filter configuration can be found in Table 3. Reconstructions were performed with an in-house implementation of the FDK (Feldkamp–Davis–Kress [10]) algorithm. Besides an outlier correction and the standard dark and flat field correction no further modifications of the projections were performed. Particularly, software corrections of beam

Table 1
Detailed specifications of the detector from Perkin Elmer [9] and the linear accelerator from U.S. Photon Service employed in the MeV CBCT setup used in this work.

XRD 1621 AN14 ES	
Manufacturer	Perkin Elmer
Pixel matrix	2048 × 2048
Pixel pitch	200 µm
Area	409.6 ×409.6 mm^2
Scintillator	DRZ-Plus
	208 µm Gd_2O_2S:Tb
Radiation energy	40 keV–15 MeV
Pulstar Linac - PSL-6D	
Manufacturer	U.S. Photon Service Inc.
Linac Design	2998 MHz (S-Band)
Electron Beam Energy	4 MeV and 6 MeV
Maximum Dose Rates	4 Gy/min at 4 MeV
at 1 m distance	8 Gy/min at 6 MeV
Target material	Tungsten
Focal spot size	2.0 mm

Table 2
Acquisition parameters of the measurements.

X-ray Source - Pulstar Linac PSL-6D		
Energy	[MeV]	6.0
Frequency	[pps]	125
Dose rate at 1 m distance	[mGy/s]	94
Detector - XRD 1621 AN14 ES		
Gain	[pF]	0.5
Binning mode		no binning
Integration time per frame	[ms]	1450–2000

Table 3
Filter configurations and corresponding integration times.

Material	Thickness	Placement	Int. time per frame
None	–	–	1500 ms
Copper (Cu)	2 mm	Detector	1500 ms
Copper (Cu)	5 mm	Detector	1450 ms
Lead (Pb)	2 mm	Source	1650 ms
Lead (Pb)	2 mm	Detector	2000 ms
Tungsten (W)	1 mm	Source	1600 ms
Tungsten (W)	1 mm	Detector	1900 ms
Copper & Tungsten	2 mm & 1 mm	Detector	1600 ms

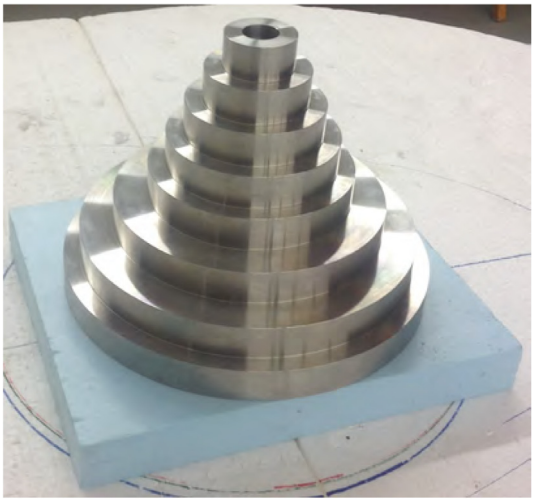

Fig. 2. Step cylinder (Stainless Steel, X5CrNi189, $\rho = 7.9\ \mathrm{g/cm^3}$) used for the filter investigations.

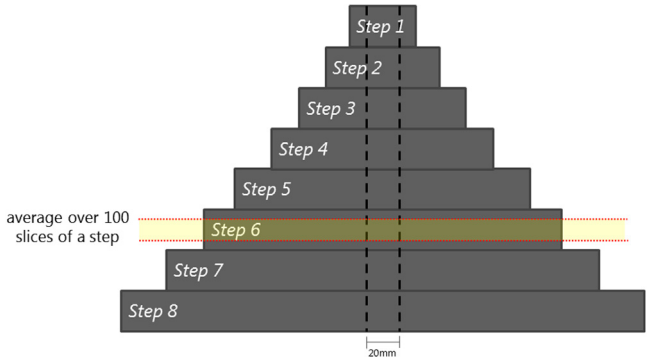

Fig. 3. Schematic drawing of the test object.

Table 4
Particles and physical interactions implemented in the GEANT4 MC simulations.

Particle	Process	Library
Photon	Photoelectric Effect	G4PenelopePhotoElectricModel
	Compton Scattering	G4PenelopeComptonModel
	Pair Production	G4PenelopeGammaConversionModel
	Rayleigh Scattering	G4PenelopeComptonModel
Electron	Ionization	G4PenelopeIonisationModel & G4UniversalFluctuation
	Bremsstrahlung	G4PenelopeBremsstrahlungModel
	Multiple Scattering	LowEnergyMultipleScattering
Positrons	Ionization	G4PenelopeIonisationModel & G4UniversalFluctuation
	Bremsstrahlung	G4PenelopeBremsstrahlungModel
	Multiple Scattering	LowEnergyMultipleScattering
	Annihilation	G4PenelopeAnnihilationModel

hardening and ring artefacts were ignored to be able to directly study the effect of each hardware configuration on the reconstructed volume.

3. MC simulation setup

In addition to the measurements described in the previous section, a set of MC simulations of the step cylinder in the MeV CBCT setup was performed. These simulations aim to deepen the understanding of the physical interactions present in the filter measurements. Specifically the change of the X-ray spectrum, when transmitted through the object is of interest here. Moreover, the effect of the detector sided filtration on the detection efficiency can be examined.

For the X-ray simulations, GEANT4 was chosen as a framework [11]. The GEANT (Generation and Tracking) framework was developed at CERN for the simulation of particle transport and interactions in matter. The fourth version, so-called GEANT4, is based on object oriented C++ programming. GEANT4 simulations cover single particle transport, which means the particles are tracked through the system individually. As a result, no interactions between two particles can be simulated. The version of GEANT4 used in this work is 4.9.6. For the physical interaction cross sections the low energy electromagnetic library EMPenelope is used. The various physical interactions and corresponding particles used in the MC simulations can be found in Table 4.

As discussed previously in [12,13] a pre-simulated spectrum of the linear accelerator is used as an input for the MC simulations. The simulations aim to understand the scatter-to-primary ratio as well as the spectral behaviour of the X-ray beam exiting the step cylinder object. Additional simulations investigate the energy dependent sensitivity of the detector with and without detector sided filtration. This sensitivity is quantified by the so-called quantum absorption efficiency (QAE), which measures the ratio of detected photons with respect to the total number of photons incident on the detector:

$$\mathrm{QAE}(E) = \frac{\text{Number of detected photons}(E)}{\text{Number of simulated photons}(E)}$$

Here, E denotes the energy of the simulated primary photons.

4. Experimental results

In order to compare the results of the different filter configurations detailed in Table 3 each scan was reconstructed with the same parameters. For the various reconstructed volumes the different steps of the step cylinder were extracted and compared. A set of 100 slices per step were averaged as shown in Fig. 3 and the radial profile of the grey value was extracted. A comparison of the reconstructed slices for the various cylinder steps will give insights into the behaviour of the detector filter with respect to the set of object transmission lengths presented here. Moreover, a direct comparison of the same filter material and size positioned at the source and the detector will demonstrate the effectiveness of the detector filter concept over the commonplace method of pre-filtered X-ray spectra.

In order to quantify the efficiency of the different filters, cupping and contrast will be evaluated. Both values can be extracted from the radial profiles for each cylinder step and filter configuration respectively. The cupping effect will be determined by comparing the lowest grey value corresponding to steel with the highest grey value in the same slice. The contrast of the inner hole with respect to the adjacent material is computed. Fig. 4 shows an illustrative radial profile and the corresponding formulas of both values.

4.1. Various detector sided filtrations

Fig. 5 shows a comparison of the unfiltered and the tungsten filtered reconstructed slices of the step cylinder. CT-Slices of steps 2, 4 and 6 according to Fig. 3 are depicted. The effect of the filter on the cupping is clearly visible. Particularly for the larger cylinder steps, the significant decrease in the grey value variation typical for cupping artefact can be observed.

Fig. 6 shows the reconstructed slice of step 6 of the steel step cylinder for all detector sided filter configurations in Table 3. At these large object transmission lengths, detector filter configurations that are either long or have higher density seem to be favoured. Qualitatively, the 5 mm copper filter reduces the cupping artefacts equally as good as the thinner and denser 2 mm lead filter. However, the contrast of the inner hole with respect to the material seems to be better for the lead and tungsten filter configuration compared to the copper filters.

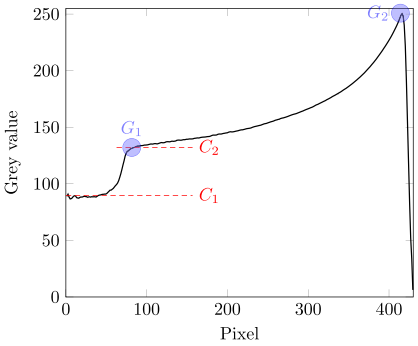

$$\text{Cupping} := \frac{G_2 - G_1}{G_2}$$

$$\text{Contrast} := \frac{C_2 - C_1}{C_1 + C_2}$$

Fig. 4. Definition of the cupping and contrast measurement at the radial profiles. Grey values G_1 and C_2 were chosen at the pixel value corresponding to the maximum of the differential of the profile at the edge. G_2 was chosen as the maximum grey value of the radial profile. C_1 is calculated as the average of the first 50 pixel values of the radial profile.

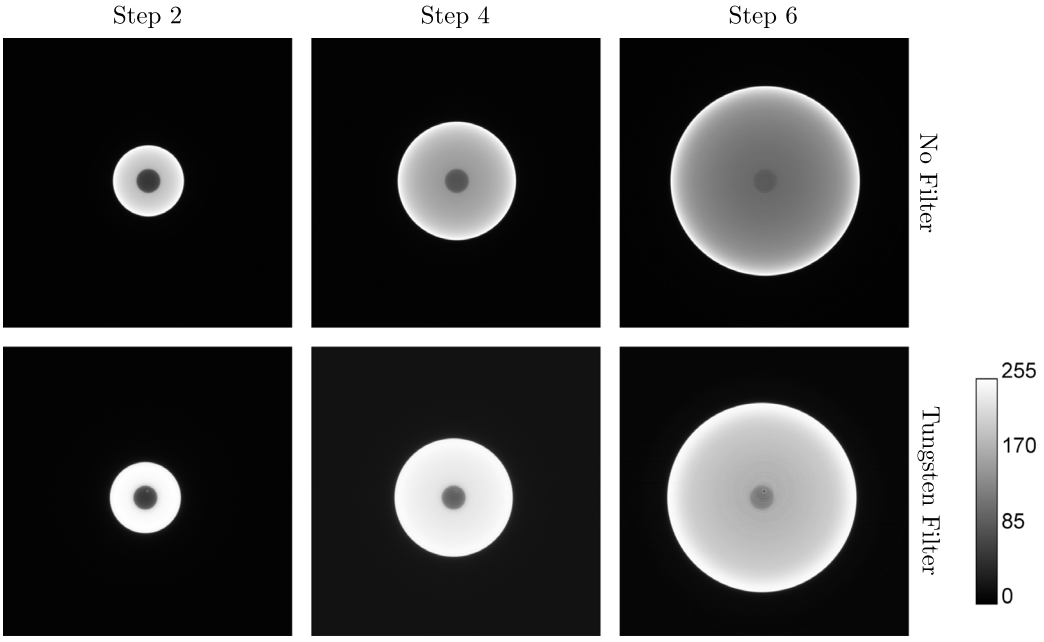

Fig. 5. Reconstructed slices for the configuration without filter (top row) and the configuration with tungsten filter (bottom row) according to Table 3. Steps 2, 4 and 6 of the step cylinder as shown in Fig. 3 are depicted.

The radial profiles extracted from steps 5 and 6 of the steel step cylinder are shown in Fig. 7. Compared to the configuration without filter, all other radial profiles even out the grey values corresponding to the material significantly. Additionally, a difference in contrast, determined according to Fig. 4, can be observed.

Fig. 8 shows the resulting plots for the amount of cupping as well as the contrast per cylinder step and detector filter configuration. A decrease in contrast accompanied by an increase of cupping can be seen for all filter configurations with increasing transmission length. All filter configurations reduce the cupping artefacts compared to the configuration without filter. Moreover, the amount of cupping in the configuration measured without detector sided filters increases roughly linear with the step diameter. In contrast to this, all other configurations show a quadratic increase in cupping. It is interesting to observe, that while cupping is corrected by all filter materials studied in this work, the same is not necessarily true for signal contrast. The configuration employing a 2 mm copper filter as well as the 5 mm copper filter setup shows a worse contrast for the small filter steps compared to the non-filtered reconstructed slices. However, for larger transmission lengths, corresponding to step numbers larger than 4, image contrast is enhanced by all detector sided filtrations. Ideally, a detector configuration should decrease cupping as much as possible, while additionally providing the optimal contrast improvement. Here, the best contrast enhancement was achieved by the 1 mm tungsten filter. However, the 5 mm copper filter and the combined copper and tungsten filter, provided the optimal cupping correction depending on the step diameter. This induces, that the choice of detector sided filter material will be a trade-off and depends on the measurement task. Parameters such as the size of the sample as well as the purpose of the measurement will play a role in selecting the best fitting filter setup.

4.2. Detector-sided filtration versus source sided filtration

The studies in the previous section show the image enhancement of the reconstructions of the step cylinder for detector sided filters. However, image degrading effects such as cupping are typically already reduced by a pre-hardened beam. Here, measurements with the same filter, i.e. same material and thickness, positioned at the source and the detector are compared. Fig. 9 shows the sixth step of the step cylinder for the two configurations employing a 1 mm tungsten filter as well as the configuration without filtration. It is clearly visible, that the source filter does not reduce the cupping as much as the same configuration with a detector sided filter. Radial profiles of the reconstructed slices of step 6 of the step cylinder for the non filtered and

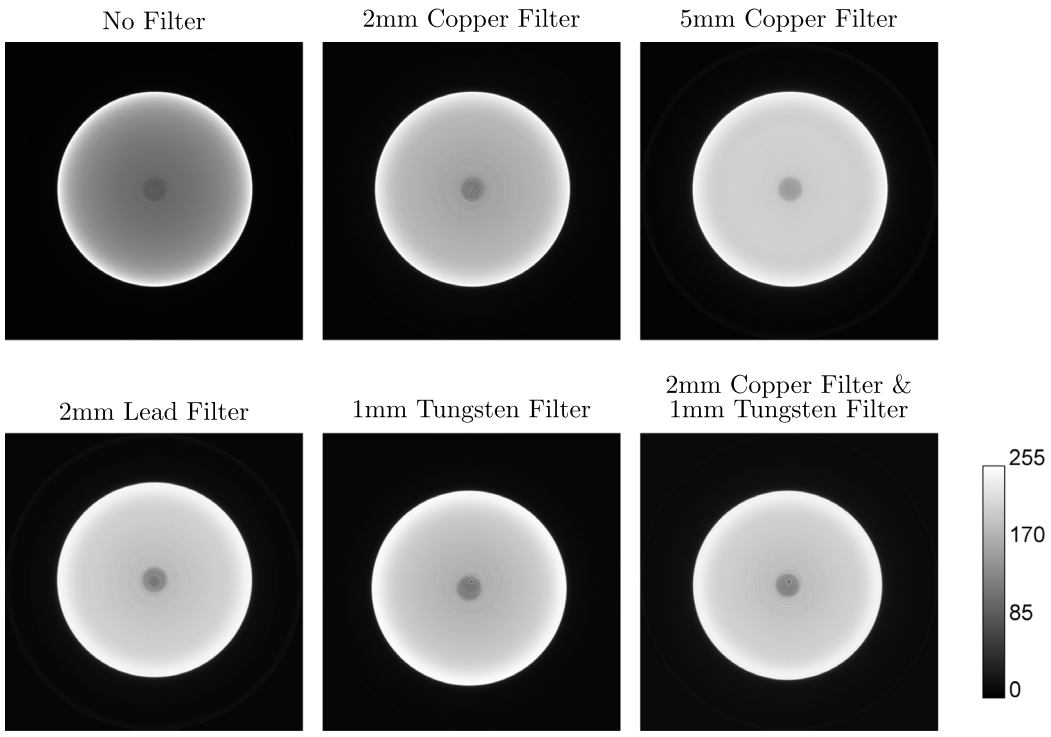

Fig. 6. Reconstruction of step 6 of the step cylinder as shown in Fig. 3 for all filters at the detector according to Table 3.

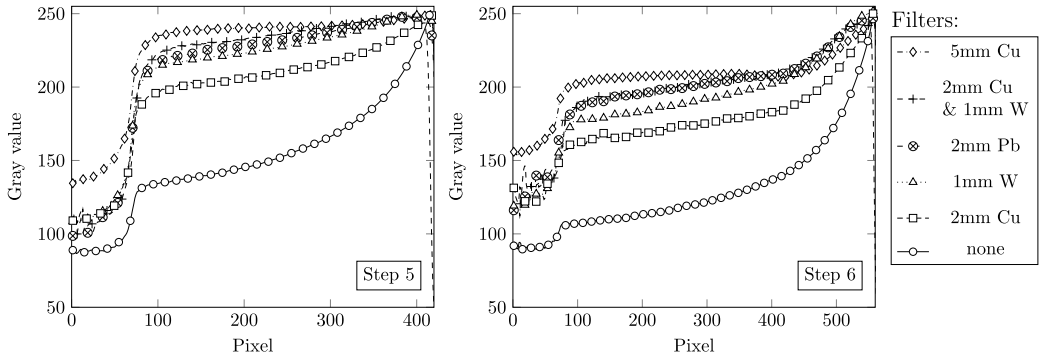

Fig. 7. Radial profiles for the reconstructed slices of step 5 and 6 of the step cylinder as shown in Fig. 3 and the non filtered and detector filtered configurations according to Table 3.

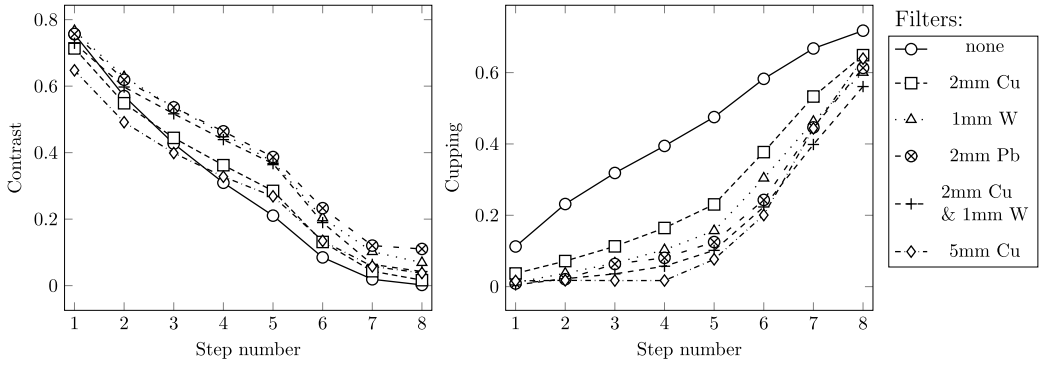

Fig. 8. Contrast and Cupping for all steps of the step cylinder as shown in Fig. 3 and the non-filtered and detector filtered configurations according to Table 3 [8].

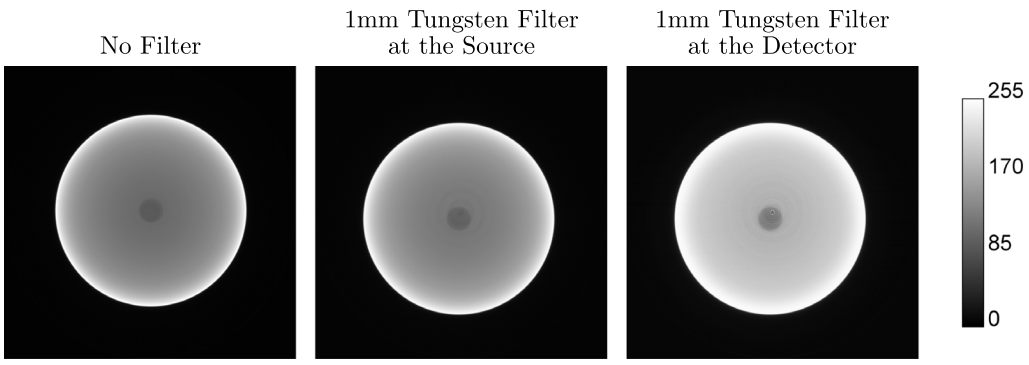

Fig. 9. Reconstruction of step 6 of the step cylinder as shown in Fig. 3 for the non filtered and tungsten filtered configurations according to Table 3.

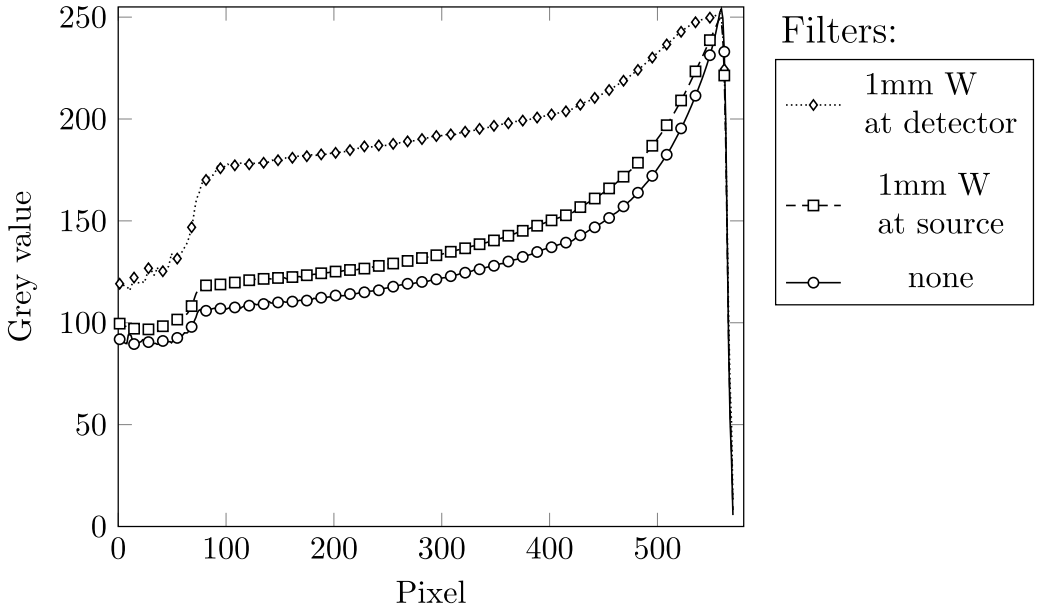

Fig. 10. Radial profiles for the reconstructions of step 6 of the step cylinder as shown in Fig. 3 for the non filtered and tungsten filtered configurations according to Table 3.

1 mm tungsten filtered configurations at the source and the detector are shown in Fig. 10. Cupping and contrast for source and detector sided filter configurations calculated according to the equations shown in Fig. 4 are compared in Fig. 11. Both tungsten and lead filtration seem to have a similar impact. The noticeable offset between the curves, particularly regarding the amount of cupping, demonstrates the overall success of detector sided filtration over source sided filtration. Moreover, it is interesting to notice that cupping seems to increase linearly for the configuration with the filter at the source following the same trend as the configuration without filter. In contrast to this, the profile corresponding to the cupping for the detector sided filter increases non-linearly with respect to the step numbers. Improvement on the contrast can only be observed for steps 3 and onwards. This difference signifies that the suggested filter method is only efficient for large transmission lengths.

The difference in efficiency between the source and detector sided filtration (cf. Fig. 11) can be explained by its relative impact on object scattered radiation. Source-sided filtration pre-hardens the beam, reducing the effect of beam hardening on the measured signal. However, image degradation caused by single and multiple scattering in the object cannot be influenced by the source filter. The filter placed at the detector can amend both effects. The filter material will filter out a large part of the scattered radiation originating from the object. At the same time, while the beam is not pre-hardened before the object, the detector sided filter will harden it before entering the detector. This leads to an equivalent effect on beam hardening as the solution provided by a source sided filter. Finally, the sensitivity of the detector for high energy radiation will increase. These properties of the detector filters will be investigated in the Monte Carlo simulations in the next section. The origin of different types of scattered radiation related to the experimental setup described in Section 2 has been investigated in previous work and published in [13] and [2].

5. Simulation results

In order to study and understand the impact of the detector filters on the radiographic images, a series of Monte Carlo simulations were performed. A first set of simulations focuses on the characterization of the X-ray beam arriving at the detector by means of its energy spectrum. The spectra of both primary radiation as well as scattered photons will be recorded for the central transmission path through each of the cylinder steps. Additionally, an energy dependent scattered to primary ratio will be computed. Fig. 12 shows the resulting spectra as well as the corresponding scatter-to-primary ratio. The spectra are plotted normalized with respect to the total intensity under the curves in order to be able to compare the profile of all spectra. The shift of the primary spectra towards higher energies for larger steps proves the formerly assumed increase in beam hardening at these transmission lengths. For steps numbers 1 to 5 the spectrum of scattered radiation is focused at small energies below 1 MeV. The relation of the amount of scattering with respect to the primary radiation at the various energies is given in the plot of the scatter-to-primary ratio shown in Fig. 12.

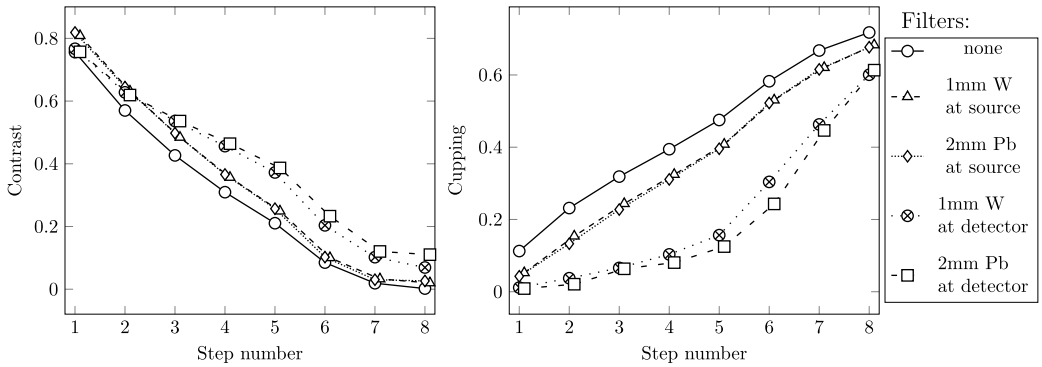

Fig. 11. Comparison of the contrast and cupping of the detector sided and their equivalent source sided configurations [8].

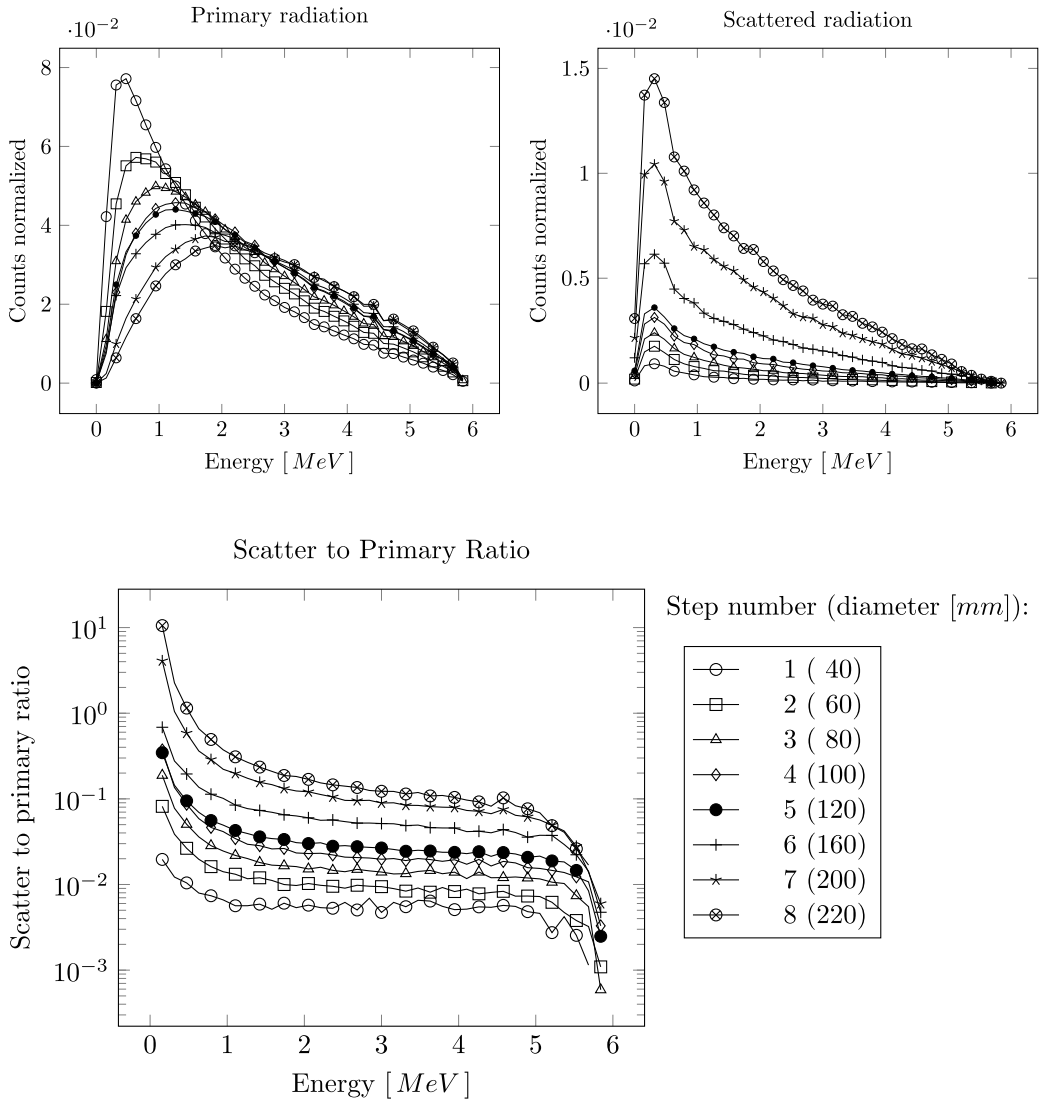

Fig. 12. Spectra and the ratio of scattered to primary radiation resulting from the step cylinder simulations. The spectra were normalized with respect to the area under their curves [8].

An overall increase in the scatter-to-primary ratio can be seen with increasing step numbers. The increase in scattered radiation at lower energies is clearly visible.

A second set of simulations investigates the change in the detector's QAE caused by the detector sided filter material. Fig. 13 shows a sketch of the setup employed in the simulations. A set of mono-energetic X-ray pencil beams are guided perpendicularly onto the detector. Here, a photon is defined to be detected, if it deposits energy in the scintillating layer of the detector. Fig. 14 shows the resulting QAE for various filter materials and thicknesses. It is obvious that the additional material

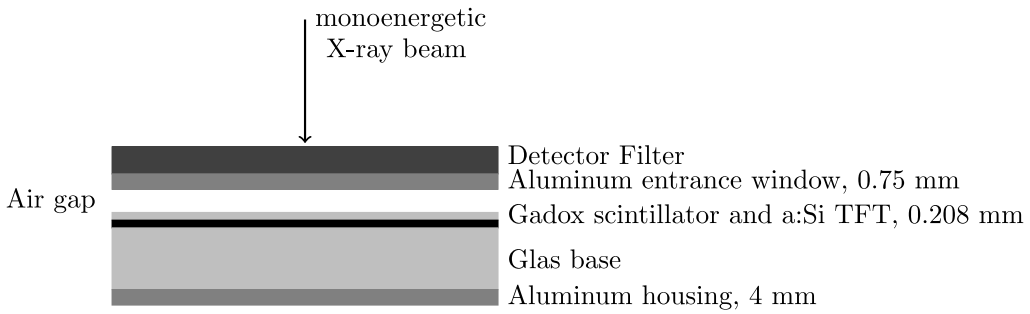

Fig. 13. Sketch of the setup for the QAE simulations. The ratio of photons depositing energy in the gadox scintillation layer with respect to the number of simulated photons will be measured. Detector filters are placed exactly in front of the aluminium entrance window of the detector.

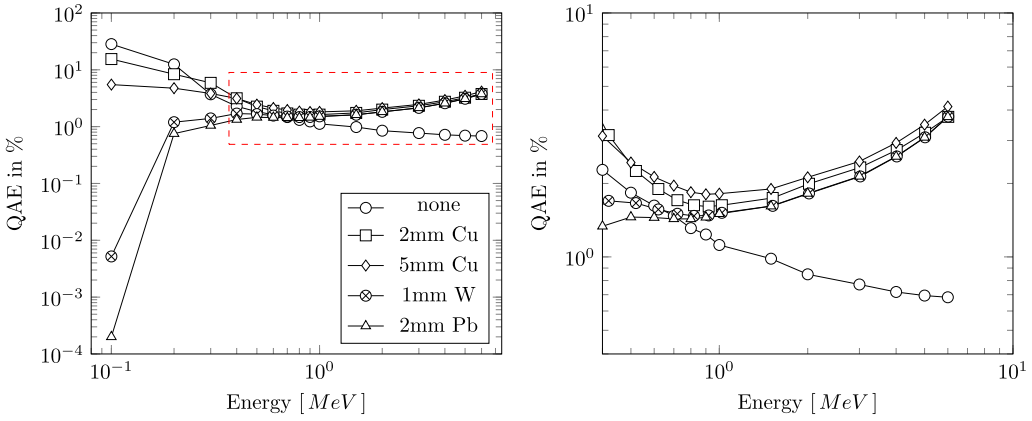

Fig. 14. Plot of the detectors QAE for various filter materials as well as the non-filtered configuration. The plot on the right shows an enhanced version of the QAE plot on the left focused on the dashed region [8].

at the detector decreases the detection of low energy photons, while increasing the detection at higher energies. In comparison with the spectra in Fig. 12, the suppression of the low energy signal arriving at the detector will decrease the impact of the shift of the mean energy that can be seen in the primary spectrum. Additionally, a large part of the scattered radiation will be cut from detection. Fig. 14 shows that the lead filter is the most effective in decreasing low energy X-ray detection, while the 5 mm Copper filter is the most effective in increasing high energy X-ray detection efficiency.

6. Discussion and conclusion

This work investigates a detector sided filter concept for contrast enhancement and cupping correction in industrial MeV CBCT. The method is evaluated using a steel step cylinder sample in order to test the effectiveness of the hardware based improvement for various material transmission lengths. The original measurement and reconstruction of the step cylinder sample exhibits large amounts of cupping and loss of contrast. These two effects can be attributed to high amounts of beam hardening as well as large scatter-to-primary ratios. The experimental results detailed in Section 4 show an improvement of the reconstructed signal for the suggested detector filter configurations over the configurations without filter. Additionally, detector filter configurations are shown to be more effective than the equivalent source filtered configurations (cf. Fig. 9). The detector sided filter configurations are particularly advantageous for large transmission lengths through the dense material as shown in Fig. 5. The improvement introduced by the detector filter manifests mainly in a reduction of cupping artefacts but also as an increase in contrast. Particularly denser filter materials lead to a significant reduction in cupping as shown in Fig. 6.

The impact on radiographic images for the various filter configurations was quantified by calculating the amount of cupping as well as contrast in the reconstructed step cylinder slices. For the filter configurations studied in this work, the 2 mm lead filter lead to the best contrast enhancement, while the 5 mm copper filter lead to better results concerning cupping artefact improvements (cf. Fig. 8). The overall improvement of the reconstruction for the detector filters compared to the configuration without filter as well as the source filter configurations can be explained by the large amount of low energy scattered radiation induced by the step cylinder. The incident X-ray signal at the detector carries information over all energies. However, at lower energies the scatter-to-primary ratio is largely enhanced as shown in Fig. 12. This means particularly at the larger transmission lengths we would like to measure the high energy photons rather than the low energy radiation in order to improve the detected signal. However it is known, that the detection rate per photon drops with the energy for the common commercial flat panel detectors. This is an effect of their thin scintillation layers. The quantum absorption efficiency of the non-filtered configuration shown in Fig. 14 proves this non-linear X-ray conversion effect. The detector filter employed here, acts as a filter for the low energy part of the incoming radiation as well as an enhancer for the detection of the high energy photons. The latter effect is caused by the Compton effect within the filter. Since the Compton scattered photons have less energy than their corresponding primary photons, the detector sided filter acts as a 'beam weakening filter'. Thus, it shifts the beam spectrum towards those energies at which the scintillator is more effective. This is shown by the simulations of the quantum absorption efficiency displayed in Fig. 14. An equal sized source sided filtration of the X-ray beam can only reduce the amount of low energy photons reaching the object. This reduces the difference in mean energy for the spectra exiting the different material transmission lengths. As a result, the source sided pre-hardening of the beam has no effect on the scattered radiation created in the object making it less effective overall.

While this work demonstrated a great success of the detector filter based correction of typical artefacts in industrial MeV CBCT, it has to be kept in mind that the filter itself acts as an additional stage in the imaging chain. The scattering in the filter material that leads to the change in QAE shown in Fig. 14 will introduce additional blur into the radiographies as well. Therefore, the investigation and quantification of the effect of the filters on the point spread function of the detector will be the focus of future work. Additionally, the impact of the filter method on multi-material samples will be of interest.

CRediT authorship contribution statement

Carina von Deschwanden: Scientific concept, Realization and analysis of all experiments, Execution of all Monte Carlo Simulations with GEANT4, Interpretation of results, Paper writing. **Richard Schielein:** Scientific concept, Discussion and contribution to the interpretation of results. **Mathieu Plamondon:** Discussion and contribution to the interpretation of results. **Jürgen Hofmann:** Installation and consulting on GEANT4 software. **Alexander Flisch:** Design and selection of reference objects for MC simulations, Design and installation of high energy X-ray setup. **Stefan Kasperl:** Guidance, contribution to interpretation of results. **Randolf Hanke:** Guidance, contribution to interpretation of results. **Alex Dommann:** Guidance, contribution to interpretation of results.

Declaration of competing interest

The authors declare that they have no known competing financial interests or personal relationships that could have appeared to influence the work reported in this paper.

Acknowledgements

This work was part of the project “Efficiency enhanced Mega Electronvolt Cone Beam Computed Tomography, Switzerland” (EMECT, SNSF project number 200021L_169412) and based on the work presented in the dissertation of Stritt [8]. The authors would like to thank the Swiss National Science Foundation (SNSF) and the German Research Foundation (DFG) for funding.

References

[1] M. Kiunke, C. Stritt, R. Schielein, F. Sukowski, A. Hölzing, S. Zabler, J. Hofmann, A. Flisch, S. Kasperl, U. Sennhauser, et al., ROSI And GEANT4–a comparison in the context of high energy X-ray physics, Nucl. Instrum. Methods Phys. Res. B 377 (2016) 50–58.

[2] C. Stritt, P. Schuetz, M. Plamondon, A. Flisch, J. Hofmann, U. Sennhauser, Quantitative untersuchung der Streubeiträge in Hochenergie-Röntgencomputertomografie, Materials Testing 58 (2) (2016) 122–126.

[3] D.A. Jaffray, J.J. Battista, A. Fenster, P. Munro, Monte Carlo Studies of x-ray energy absorption and quantum noise in megavoltage transmission radiography, Med. Phys. 22 (7) (1995) 1077–1088.

[4] H. Gustafsson, P. Vial, Z. Kuncic, C. Baldock, P.B. Greer, EPID Dosimetry: Effect of different layers of materials on absorbed dose response, Med. Phys. 36 (12) (2009) 5665–5674.

[5] L.N. McDermott, R.J.W. Louwe, J.-J. Sonke, M.B. Van Herk, B.J. Mijnheer, Dose–response and ghosting effects of an amorphous silicon electronic portal imaging device, Med. Phys. 31 (2) (2004) 285–295.

[6] A.K. Hunter, W.D. McDavid, Characterization and correction of cupping effect artefacts in cone beam CT, Dentomaxillofacial Radiol. (2014).

[7] K. Schiebold, Zerstörungsfreie Werkstoffprüfung-Durchstrahlungsprüfung, Springer-Verlag, 2014.

[8] C. Stritt, Assessment and Correction of Image Degradation in MeV Cone Beam Computed Tomography, PhD thesis, ETH Zurich, 2017.

[9] PerkinElmer, XRD series product note.

[10] L.A. Feldkamp, L.C. Davis, J.W. Kress, Practical cone-beam algorithm, J. Opt. Soc. Amer. A 1 (6) (1984) 612–619.

[11] S. Agostinelli, J. Allison, K. Amako, J. Apostolakis, H. Araujo, P. Arce, M. Asai, D. Axen, S. Banerjee, G. Barrand, et al., GEANT4—a simulation toolkit, Nucl. Instrum. Methods Phys. Res. Section A: Accelerators, Spectrometers, Detectors and Associated Equipment 506 (3) (2003) 250–303.

[12] C. Stritt, P. Schuetz, J. Hofmann, A. Flisch, U. Sennhauser, Quantitative assessment of scattering contributions in MeV-Industrial X-ray computed tomography, in: Proceedings of the 11th European Conference on Non-Destructive Testing, 2014.

[13] C. Stritt, M. Plamondon, J. Hofmann, A. Flisch, U. Sennhauser, Performance quantification of a flat-panel imager in industrial mega-voltage X-ray imaging systems, Nucl. Instrum. Methods Phys. Res. A (2016).